12-2018

Epoxy Interlocking: A Novel Approach to Enhance FRP-to-concrete Bond Behavior

Cheng Jiang
Hong Kong Polytechnic University

Baolin Wan
Marquette University, baolin.wan@marquette.edu

Yu-Fei Wu
RMIT University

John Omboko
Marquette University

Epoxy Interlocking: A Novel Approach to Enhance FRP-to-concrete Bond Behavior

Cheng Jiang[1]
The Hong Kong Polytechnic University, Hong Kong Special Administrative Region
Baolin Wan
Marquette University, Milwaukee, WI
Yu-Fei Wu
School of Engineering, RMIT University, Melbourne, VIC 3000, Australia
John Omboko
Marquette University, Milwaukee, WI

Highlights

- A novel epoxy interlocking approach is proposed to enhance FRP-to-concrete bond.
- Partial interaction of epoxy interlocking was calibrated by test results.
- An analytical method was proposed to quantify partial interaction for epoxy ribs.
- A parametric study was conducted analytically on the effects of epoxy interlocking.

Abstract

This paper presents a novel approach which can enhance the interfacial bond behavior between fiber reinforced polymer (FRP) composite material and concrete. Epoxy ribs are formed by grooving on the concrete surface before epoxy is applied. The dowel action from the epoxy ribs leads to an "epoxy interlocking" effect. The mechanism of the proposed epoxy interlocking approach was analyzed in this paper from both adhesion and interlocking aspects. Furthermore, the partial interaction of the epoxy interlocking was quantified and calibrated by experimental results. The epoxy interlocking in the tested specimens led to an 88.8% increase in bond strength on average. An analytical approach was proposed to quantify the average partial interaction for the individual epoxy ribs. The load-slip relationship for individual epoxy ribs was found to be related to concrete compression behavior. A parametric study was conducted analytically on the effects of groove depth and spacing, concrete strength and epoxy rib location. The reasonable results in the parametric study further verify the efficiency of the epoxy interlocking to enhance the bond performance between FRP and concrete.

Keywords

FRP, Concrete, Epoxy interlocking, Interfacial bond,

Nomenclature

b_c width of concrete block
b_f width of applied FRP
D distance from loaded end
d_e depth of the grooves
E_c Elastic modulus of concrete
E_f modulus of elasticity of FRP
F pull load
F_a force from adhesion
f_{co} compressive strength of concrete
F_F load of epoxy interlocking specimens
F_m force from mechanical interlocking, or dowel force
F_{max} maximum force value of force-slip relationship
F_U load of wax filled specimens
L_e effective bond length
L_f total bond length of FRP
L_r spacing of the epoxy ribs
S relative slip between FRP and concrete
$s(x)$ slip distribution along x coordinate
s_u maximum slip at loaded end (when failure)
t_f FRP thickness
x_0 location (in x coordinate) of maximum bond stress (Fig. 2c)
α a bond parameter needs to be determined in Eq. (2)
α_F obtained α value for epoxy interlocking specimens
α_U obtained α value for wax filled specimens
β a bond parameter needs to be determined in Eq. (2)
β_F obtained β value for epoxy interlocking specimens
β_U obtained β value for wax filled specimens
ε strain
ε_{co} strain when concrete stress = f_{co}
σ stress
τ_a bond stress between FRP and concrete

1. Introduction

Externally bonded (EB) fiber reinforced polymer (FRP) composite material is popular for the rehabilitation of concrete structures, largely due to its high mechanical performances and advantages in construction convenience [1], [2], [3], [4], [5], [6]. The FRP-to-concrete interfacial bond is the weakest link in this retrofitting system. It is known that there are three mechanisms, i.e., adhesion, interlocking/dowel action, and friction, to transfer the interfacial bond stresses in a composite structure combining two mechanically connected bodies. Researchers have suggested various methodologies based on these three mechanisms to enhance the FRP-to-concrete bond performance.

Adhesion is normally provided by epoxy resin as an adhesive applied between FRP and concrete. Hosseini and Mostofinejad [7], [8] increased the total adhesive area between FRP and concrete by grooving on the concrete surface before applying epoxy. However, the reliability of the adhesive works is often doubted by engineers and researchers because of the debonding issue [9]. To solve this problem, the bond behavior should be enhanced from the other two aspects: interlocking (or dowel action) and friction. FRP anchors [10], [11], [12], [13] and mechanically fastening with anchor bolts [14], [15], [16] are the most common devices used in the applications of interlocking. Zhang et al. [17] added shear keys with FRP plates to increase the interlocking effect. The anchors, however, cut fibers which lead to longitudinally splitting and/or need a related deep burrowing leading to some damage to concrete. Recently, a hybrid bonding system using mechanical fasteners [18], [19], [20], [21], [22] was proposed to generate perpendicular pressure to provide high friction between FRP and concrete, as well as interlocking by nails. Such system can improve the FRP-concrete bond significantly. However, the installation of the mechanical fasteners increases the complication of the installation process apart from the damage effect to concrete.

Because of the limitations mentioned above, this study aims to find a novel and reasonable method by a theoretical study to effectively increase the FRP-to-concrete bond behavior. A new concept of epoxy interlocking, which is an interlocking enhancement method neither cutting FRP nor severely damaging concrete, is proposed and verified by tests with analytical derivations. A parametric study was conducted analytically on the effects of groove depth and spacing, concrete strength and epoxy rib location.

2. Epoxy interlocking

Cutting FRP laminates can be avoided if the dowel action is created only in the concrete layer. There are three conditions for a dowel to work effectively: (1) the dowel should be tightly fixed on the FRP; (2) the dowel should insert into concrete for a certain depth; and (3) the strength of the dowel material should be much higher than concrete. In this study, a simple and effective concept is proposed that the adhesion level can be adjusted and improved to have “ribs”, which is similar to the deformed steel reinforcing bars. The schematic diagram is shown in Fig. 1. The “epoxy ribs” can be formed by grooving the concrete before applying epoxy resin. Both the adhesion layer and the interlocking ribs are made of epoxy resin, and the proposed approach can be considered as “epoxy interlocking”. In order to avoid the shear failure of the ribs and concrete damage, it is not necessary to have a large grooving depth. Since epoxy normally has a higher strength than concrete, it is believed that the epoxy filling in the grooves has a very limited or no damage effect on the concrete material. On the other hand, a recent work by the authors [23] shows that the existing cracks have a limited influence on the bond-slip relationship, and the shallow grooves cut on the tensile side of the reinforced concrete beam does not have significant effects on the stiffness and capacity of the FRP strengthened RC beam.

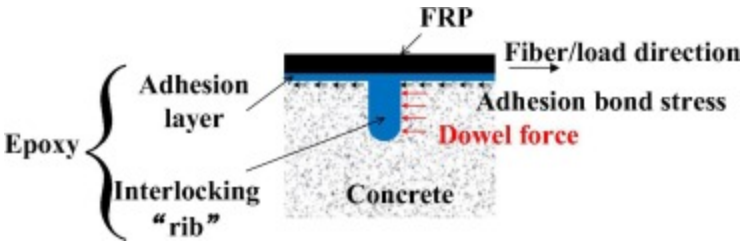

Fig. 1. Epoxy rib.

3. Bonding mechanisms

In this proposed method, only adhesion and interlocking (or dowel action) are involved in the bonding mechanisms, as illustrated in Fig. 2. The external force applied to the FRP is balanced by the sum of every mechanism's effect [9]. Therefore, the total pull load F of EB-FRP joints considering epoxy interlocking is

(1) $F = F_a + F_m$

where F_a and F_m are the forces from adhesion and mechanical interlocking, respectively.

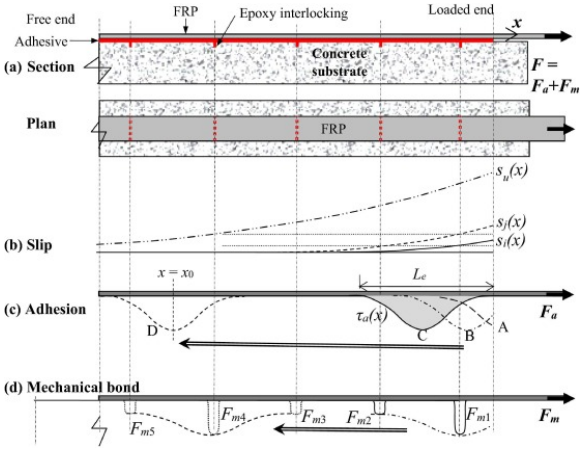

Fig. 2. Interfacial bonds.

3.1. Adhesion

Adhesive bond behavior between FRP and concrete has been extensively investigated over the last two decades. FRP tends to move, or slip, relative to the concrete substrate when subjected to a pull load F, as shown in Fig. 2a. The adhesive resistance of the interface is mobilized by the FRP slipping, with a typical bond stress τ_a vs. slip s relationship (Fig. 3a) [24]. When the loaded end slip increases from zero to the maximum slip, s_u, as shown by the slip distribution $s(x)$ in Fig. 2b, the adhesive bond stress develops gradually from state A to C, as shown in Fig. 2c, where a full bond stress block is developed with τ_a equal to 0 at the loaded end. Further pulling after state C will simply move the bond stress block to the free end as shown by state D. The area on the right side of stress block D has been fully debonded [24]. Therefore, the total adhesive bond, F_a, reaches its peak at state C and remains constant thereafter. The length of the bond stress block corresponding to state C in Fig. 2c, L_e, is the effective length of adhesive bond. Increasing the total bond length (L_f) beyond L_e cannot increase F_a. L_e is usually in the magnitude of 100 mm, depending on the properties of the joint such as FRP stiffness and concrete strength [25], [26], [27], [28]. Therefore, the capacity of the adhesive bond is very limited.

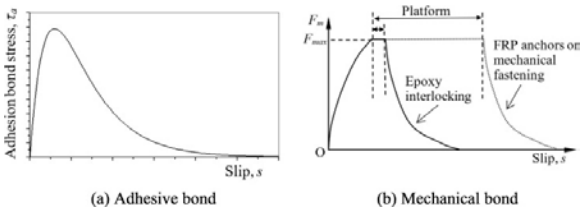

Fig. 3. Partial interaction relationships.

3.2. Dowel action

The dowel force of the epoxy ribs is significantly different from those with FRP anchors and mechanical fastening. For FRP anchors and mechanical fastening, the dowel action occurs in both anchor-to-FRP interface and anchor-to-concrete interface, as shown in Fig. 4. Because of the relatively deep anchor, the interlocking effect in concrete (dowel force 2 in Fig. 4) is much higher than that in the FRP laminate (dowel force 1 in Fig. 4). Therefore, the failure mode of the FRP anchor/mechanical fastening system is normally either the shear failure of the anchors or the cutting failure of FRP laminates, which is also called sustained bearing failure [14]. Hence, the dowel action of FRP anchors and mechanical fastening largely depends on the anchor-to-FRP force which can lead to a large platform in a local load-slip relationship [19], [29], as illustrated by the dotted line in Fig. 3b.

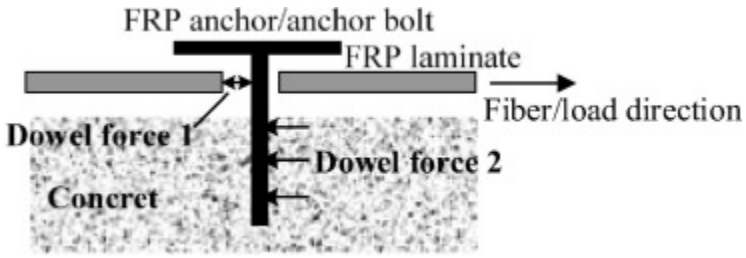

Fig. 4. Dowel force of FRP anchor and mechanically fastening.

For the epoxy interlocking case, however, only the interlocking effect in concrete, which is the dowel force shown in Fig. 1, exists. Under a pull load, FRP tends to move relatively to the concrete substrate with dragging the epoxy ribs. The concrete at the side of pull force has the dowel force to resist such pushing pressure. Eventually, the concrete would crush and be pulled off with the epoxy layer. Therefore, the partial load-slip relationship of epoxy interlocking should have a much shorter platform as illustrated in Fig. 3b (solid line), and may be related to concrete compressive behavior [30]. The development of mechanical bond is similar to the adhesion bond with a movement from the loaded end to the free end (Fig. 2d). The partial interaction of the epoxy interlocking (Fig. 3b) can be quantified and calibrated by experiments as described in the following sections.

4. Calibration by experiments

To verify the proposed concept and to calibrate the effect of epoxy interlocking, an experimental program was conducted. Three EB-FRP joints with epoxy interlocking (Fig. 5a) were prepared by grooving before applying FRP. On the other hand, three additional EB-FRP joints with wax filled grooving (Fig. 5b) were undertaken for the sake of comparison. Such type of comparison was adopted in order to investigate the interlocking effect independently. The specimen details are illustrated in Table 1 and Fig. 6. The 28-day compression strength of the concrete substrates was 34.5 MPa obtained by compression tests on cylinder specimens sized 150 mm (diameter) × 300 mm (height). The nominal thickness, ultimate strength, ultimate strain and tensile modulus of

carbon FRP (CFRP) plates were 1.5 mm, 2790 MPa, 1.8%, and 155 GPa, respectively, which were provided by the manufacturer.

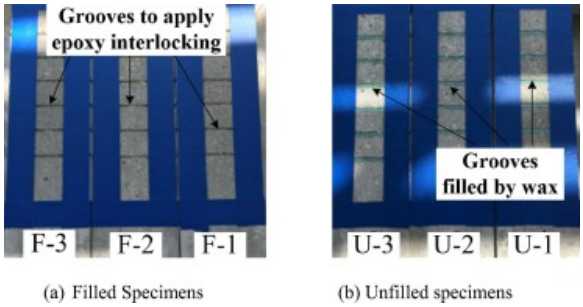

Fig. 5. Grooving on concrete.

Table 1. Specimen detail and test results of EB-FRP joints.

Specimen ID	Epoxy interlocking/grooving				Peak load (kN)	α (mm)	β (mm)
	Width (mm)	Spacing (mm)	Depth d_e (mm)	Filling material			
U-1	3	50	4.9	Wax	29.74	0.1115	43.11
U-2			5.0		31.50		
U-3			5.0		37.69		
F-1	3	50	4.8	Epoxy	65.02	0.1949	39.47
F-2			4.9		64.87		
F-3			5.0		57.02		

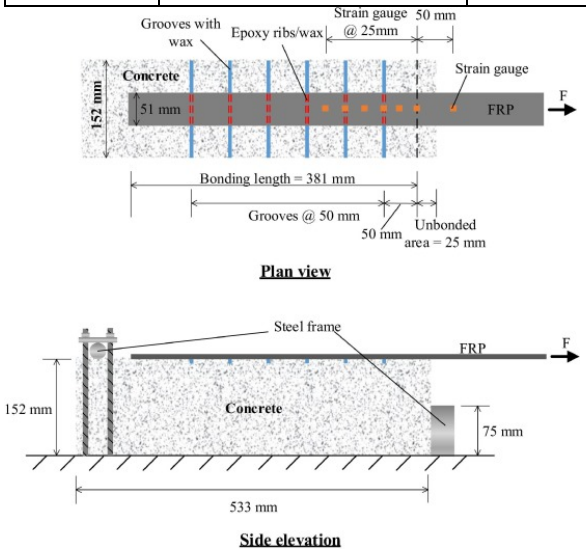

Fig. 6. Sketch of the specimen and test setup.

Grooves with 3 mm in width and 5 mm in depth of all the concrete substrate were cut by a concrete saw after roughening the concrete surface by mechanical grinding. Three of the specimens (U-1, U-2 and U-3) were filled by soft wax to avoid the penetration of applied epoxy. The wax filling was also carried out at the edges of grooves in the epoxy interlocking specimens (F-1, F-2 and F-3) where were not be covered by CFRP. Hence, the epoxy ribs had the same width with FRP.

The single shear pull-out test with a loading rate of 0.0127 mm/s was adopted to evaluate the bond behaviors of the EB-FRP joints in this work (Fig. 7). Seven conventional electric strain gauges were mounted on the FRP surface for each specimen to measure the FRP strain, as shown in Fig. 6. One linear variable differential

transformer (LVDT) was mounted on the concrete substrate to measure the relative displacement between concrete and FRP at the loaded end.

Fig. 7. Specimen under testing.

All specimens were loaded until a sudden failure with pulling off a thin layer of concrete skin from the concrete substrate. Fig. 8 shows the typical failure modes of the two types of EB-FRP joints. It can be observed from Fig. 8 that the thickness of damaged concrete of epoxy interlocking specimens was significantly greater than that of the wax filled ones. More concrete was crushed close to the epoxy ribs. The tested load-displacement curves at the loaded end are plotted in Fig. 9. More detail information of the experimental program can be found in [31].

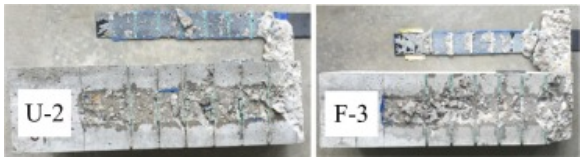

Fig. 8. Typical failure modes [31].

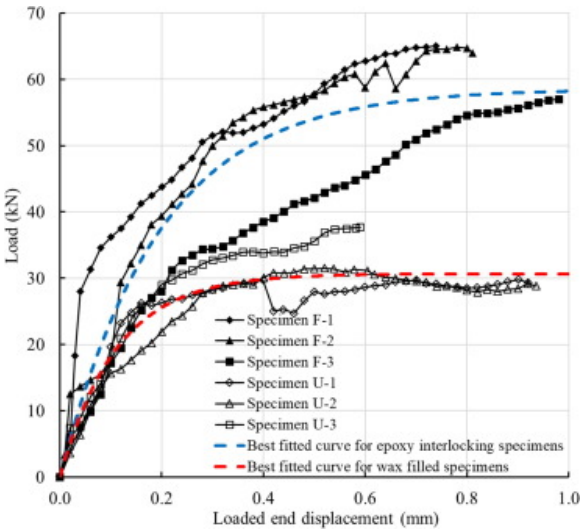

Fig. 9. Load-displacement curves [31].

5. Discussion and validation

5.1. Effect of epoxy interlocking

For wax filled specimens (i.e., U-1, U-2 and U-3), the global load-displacement behaviors show the similar responses with a 33.0 kN of average bond strength. Its bond strength is similar to that of the EB-FRP joints without grooving [31], [32]. For the epoxy interlocking specimens (i.e., F-1, F-2 and F-3), the average bond strength is 62.3 kN which shows a stable level and is 88.8% higher than that of the wax filled ones. The load-displacement curves of epoxy interlocking specimens, however, show a large scatter in Fig. 9. The large scatter

exists mainly due to the non-uniformity of concrete material and the effect of epoxy interlocking. It is known that concrete is a non-uniform composite material. Wall effect [33], [34] of concrete causes smaller aggregates to concentrate near the surface of the concrete specimen, which leads to higher non-uniformity of concrete near the epoxy ribs. Meanwhile, not all epoxy ribs contribute the same amount of resistance when the debonding crack propagates from the loaded end to the free end. Therefore, the load-displacement curves show large differences in the three specimens. While the bond strengths are similar because there are totally six ribs in each specimen and in consequence, the overall interlocking effect should not have a large variation.

5.2. Mechanical evaluation of epoxy interlocking

An analytical approach is proposed in this study to evaluate and quantify the effect of individual epoxy interlocking. A widely adopted bond-slip model and its analytical solution for load-displacement relationship are used and shown in Eqs. (2), (3), respectively [23], [24], [26], [35], [36], [37], [38], [39].

(2) $\tau(s) = \frac{E_f t_f \alpha}{\beta^2} e^{-\frac{s}{\alpha}} \left(1 - e^{-\frac{s}{\alpha}}\right)$

(3) $F = E_f t_f b_f \frac{\alpha}{\beta} \left(1 - e^{-\frac{s_0}{\alpha}}\right)$

where E_f, t_f, and b_f are the modulus of elasticity, thickness and width of the FRP plate, respectively; s_0 is the slip at the loaded end. There are two unknown parameters, α and β, in the bond-slip relationship, which govern the shape of the bond-slip curve. The unknown coefficients α and β can be obtained by a numerical nonlinear regression analysis using Eq. (3) to fit the experimental load-displacement curves of specimens.

The best fitted load-displacement curves regressed by Eq. (3) plotted in Fig. 9 are used to study the average effect due to the non-uniformity of surface concrete as mentioned above. The bond-slip relationships from both direct measurement (calculated from strain gauge data) and indirect analytical solutions (regression from load-displacement curves using Eqs. (2), (3)) are illustrated in Fig. 10.

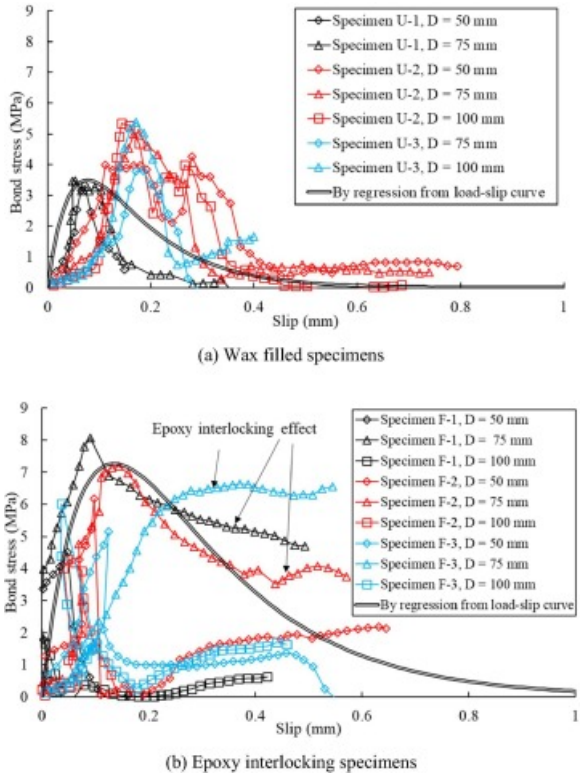

Fig. 10. Bond-slip relationship [31] (D is the distance from the loaded end, D = 75 mm refers to the epoxy rib locations).

Based on Eq. (1) and Fig. 2, the load due to mechanical interlocking can be studied independently by

(4a) $F_m = F - F_a = F_F - F_U$

where F_F and F_U are the load values of specimens with and without epoxy interlocking, respectively. Substituting Eq. (3) into Eq. (4a) yields

(4b) $F_m = E_f t_f b_f \left[\frac{\alpha_F}{\beta_F}\left(1 - e^{-\frac{s}{\alpha_F}}\right) - \frac{\alpha_U}{\beta_U}\left(1 - e^{-\frac{s}{\alpha_U}}\right)\right]$

in which α_F, β_F, α_U and β_U are obtained α and β values for epoxy interlocking specimens and wax filled specimens, respectively, which are listed in Table 1. The results of F_m by test data and Eq. (4b) are plotted in Fig. 11. Both the error evaluation index R^2 and integral absolute error (IAE) [40], [41], [42] show good agreement in Fig. 11.

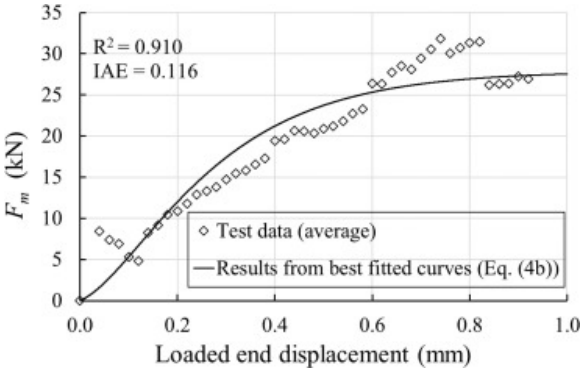

Fig. 11. Mechanical interlocking force.

When the bond slip model of Eq. (2) is adopted, the slip distribution should follow Eq. (5) [24], [38]:

(5) $s(x) = \alpha \ln\left(1 + e^{\frac{x - x_0}{\beta}}\right)$

where x_0 is the location of maximum bond stress (Fig. 2c) that moves from infinity to zero when loading.

Let the closest rib to the loaded end to be No. 1 rib, and the farthest one to be No. 6 rib. Accordingly, for a given loaded end slip, e.g., slip distribution $s_i(x)$ in Fig. 2b, the slip values for each epoxy rib are fixed as s_{i1} to s_{i6}. When the partial interaction relationship of every epoxy rib follows the load-slip relationship as:

(6) $F = f(s)$

For $s_i(x)$ of slip distribution in Fig. 2b, the corresponding total dowel force F_{mi} is

(7a) $F_{mi} = \sum_{n=1}^{6} f(s_{in})$

Furthermore, as Eq. (5) is a continuous mathematic function, there must exist another slip distribution $s_j(x)$ with $s_{j2} = s_{i1}$, $s_{j3} = s_{i2}$, $s_{j4} = s_{i3}$, etc. The corresponding total dowel force F_{mj} can be calculated as

(7b) $F_{mj} = \sum_{n=1}^{6} f(s_{jn}) = f(s_{j1}) + \sum_{n=1}^{5} f(s_{in}) = f(s_{j1}) + F_{mi} - f(s_{i6})$

In Eq. (7b), $f(s_{i6})$ is infinitesimal of high order because the slip at the last rib is very close to zero unless at the stage of specimen failure. Therefore, Eq. (7b) can be changed to be(8)fsj1≅Fmj-Fmiwhere F_{mi} and F_{mj} values can be found in Fig. 11 (or Eq. (4b)). In this way, Eq. (6) can be plotted point by point in Fig. 12a.

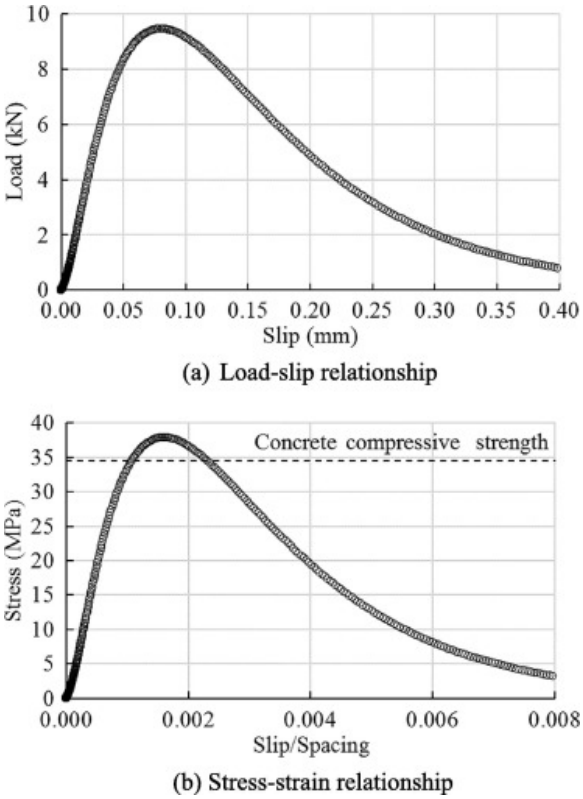

Fig. 12. Partial interaction relationship of epoxy rib interlocking.

The load-slip relationship in Fig. 12a shows a good agreement with the guessed relationship in Fig. 3b by reasonable analysis. To further study Fig. 12a, if the ordinate change to stress by dividing the cross-sectional area of one epoxy rib (= $b_f d_e$ where d_e are groove depth), and let the abscissa change to strain by dividing the groove spacing, the curve becomes very similar to the concrete compressive stress-strain relationship. This interesting phenomenon is quite reasonable because the dowel force comes from the resistance of concrete subjected to compression. The peak stress in Fig. 12b is a little higher than concrete compressive strength obtained by cylinder testing because the concrete, which is close to the epoxy rib in the specimen, is confined by the surrounding concrete.

6. Parametric study

Based on the analytical model presented above, if the partial interaction relationship (or local load-slip relationship) of the epoxy ribs is known, the global performance (e.g., load-displacement curves for FRP-concrete pull-out test) can be subsequently derived. The effects of groove depth, groove spacing, concrete strength and epoxy rib locations are further discussed in this section through a parametric study by analytical modeling. A typical FRP-to-concrete joint specimen was used in the parametric study with b_f = 50 mm, b_c = 150 mm, E_f = 155 GPa, t_f = 1.5 mm, and L_f = 350 mm. Other parameters (i.e., concrete strength and groove details) are controlled or changed, which will be further discussed. In the parametric study, it is assumed that the specimen fails with concrete crushing/peeling off, without damage of epoxy ribs. The width of the epoxy ribs is 3 mm which is equal to the thickness of concrete saw blade, is kept constant.

As discussed above, the local load-slip relationship of epoxy ribs is highly related to the concrete compressive stress-strain relationship. A classic model for concrete stress (σ)-strain (ε) relationship proposed by Popovics [43] is adopted in this study to predict the partial load-slip relationship of individual epoxy ribs. The governing function of concrete stress-strain model is

(9) $\frac{\sigma}{f_{co}} = \frac{x \cdot a}{a-1+x^a}$

where x is the normalized strain which is given by $x = \varepsilon/\varepsilon_{co}$; a is determined by

(10a) $a = \frac{E_c}{E_c - f_{co}/\varepsilon_{co}}$

where E_c and ε_{co} are the concrete elastic modulus and strain value when $\sigma = f_{co}$, respectively. E_c and ε_{co} depend on the concrete compressive strength, f_{co}, and can be calculated by using Eq. (10b) [44] and Eq. (10c) [45], respectively.

(10b) $E_c = 4730\sqrt{f_{co}}$

(10c) $\varepsilon_{co} = (0.71 f_{co} + 168) \times 10^{-5}$

After calculating the compressive stress-strain relationship of concrete, the partial load (F_r)-slip (s_r) relationship for individual epoxy ribs can be converted by $F_r = \sigma \cdot b_f \cdot d_e$ and $s_r = \varepsilon \cdot L_r$, where L_r is the spacing of the epoxy ribs or grooves, as discussed in the previous section.

The relationship between the applied load and the slip at the loaded end for the FRP-to-concrete pull-out tests is analytically derived by the steps shown in the flowchart (Fig. 13). It is noted that for specimens with epoxy interlocking, the nearest epoxy rib to the loaded end is located with a distance of L_r from the loaded end.

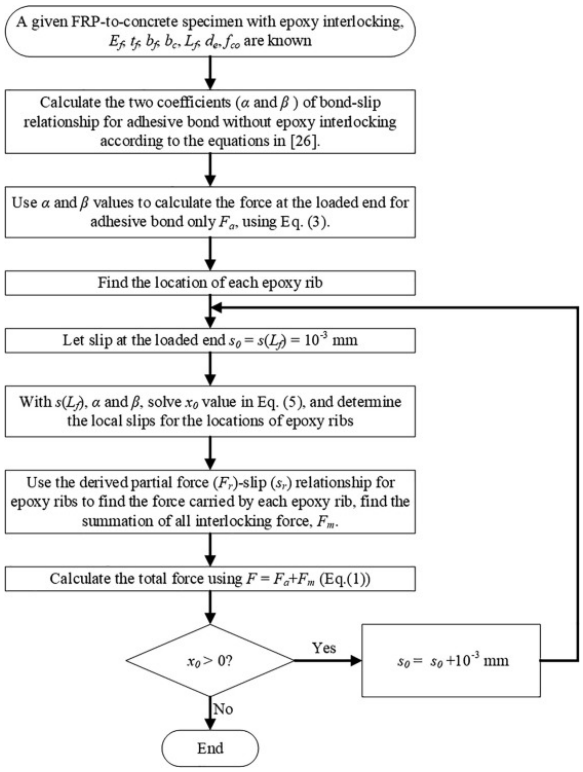

Fig. 13. Flowchart for load-displacement derivation.

6.1. Effect of groove depth

Specimens with f_{co} = 35 MPa and L_r = 50 mm (i.e., six ribs located at distances of 50 mm, 100 mm, 150 mm, 200 mm, 250 mm, and 300 mm, respectively, from the loaded end) are studied in this work. Normally, an RC beam required strengthening has the concrete cover of around 20 mm or even less. Deeply grooving may cut the internal steel and significantly damage the concrete. Hence, three different groove depths of 3 mm, 5 mm and 7 mm are used to study the groove depth effect. According to the analytical derivation discussed above the calculated partial load-slip relationships and the load-displacement curves at the loaded ends are plotted in Fig. 14a and b, respectively.

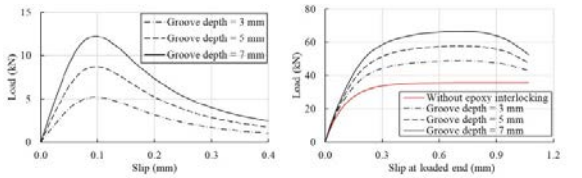

(a) Partial load-slip relationship for epoxy ribs (b) Load-displacement curves at loaded ends

Fig. 14. Effect of groove depth.

It is obvious that the partial load-slip relationship for individual epoxy ribs enhances significantly with the increasing groove depth, because greater cross-sections of concrete are involved to contribute the resistance for the epoxy ribs. The deeper epoxy ribs lead to higher loads at the loaded end which can be seen in Fig. 14b. In the load-displacement curves, the force drops at the end are due to the rapid decreasing of the contributions by epoxy ribs. Before debonding failure of the specimen, the shear stress concentrates at the free end of FRP and the epoxy ribs carry only a small amount of force with large local slips, as shown in Fig. 14a. Therefore, at the end of load-displacement curve before failure, the force reduces to a value close to that of the normal bonding (without epoxy interlocking) specimen.

6.2. Effect of groove spacing

Similarly, let f_{co} = 35 MPa and d_e = 5 mm, three different conditions for groove spacing (i.e., 10 ribs @ 30 mm, 6 ribs @ 50 mm, and 3 ribs @ 100 mm) are used in the parametric study. The calculated partial load-slip relationships and load-displacement curves at the loaded ends are plotted in Fig. 15. With the same force applied at an epoxy rib, the rib in the specimen with greater groove spacing has the greater deformation, as shown in Fig. 15a. The reason is that the larger length of concrete with the same stress-strain relationship results in a higher deformation with a fixed strain.

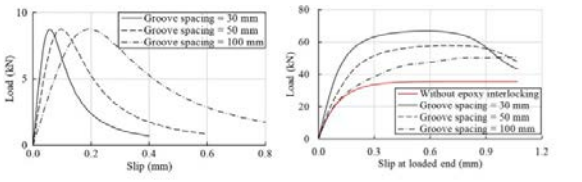

(a) Partial load-slip relationship for epoxy ribs (b) Load-displacement curves at loaded ends

Fig. 15. Effect of groove spacing.

In the load-displacement curves at the loaded ends (Fig. 15b), the curve for the specimen with a smaller groove spacing, or with more epoxy ribs, drops more significantly at the end before debonding failure. This phenomenon is reasonable because the decreasing of the contributions by epoxy ribs at the end stage are different for various groove spacings. For the specimens with shorter groove spacing, or more epoxy ribs, the residual force for a large slip at one epoxy rib is much lower than that of specimens with greater groove spacing, as illustrated in Fig. 15a.

6.3. Effect of concrete strength

In order to study the effect of concrete strength independently, the groove depth and spacing are fixed to be 5 mm and 50 mm (6 ribs @ 50 mm), respectively. Four compressive strengths of concrete are used with 35 MPa, 50 MPa, 65 MPa, and 80 MPa, respectively. The partial load-slip relationships for individual epoxy ribs and load-displacement curves at the loaded ends for the specimens with different concrete strengths are plotted in Fig. 16. It is obvious in Fig. 16a that different concrete strengths lead to different partial load-slip relationships due to the different stress-strain relationships of concrete.

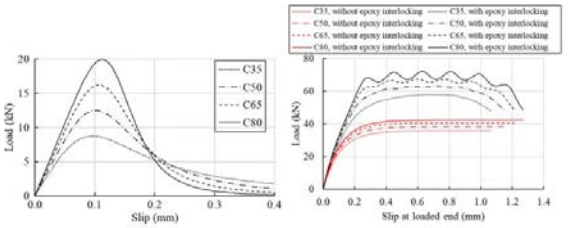

(a) Partial load-slip relationship for epoxy ribs (b) Load-displacement curves at loaded ends

Fig. 16. Effect of concrete strength.

In terms of the load-displacement relationship at the loaded end, a very reasonable phenomenon – "force fluctuations" is shown in the specimens with higher concrete grades. Such fluctuations of force appear due to the mechanical interlocking, especially for the higher concrete strength with more significant interlocking effects. The interfacial shear stresses develop gradually from the loaded end to the free end, and the ribs also start and finish its load resistance one by one from the loaded end to the free end, as illustrated in Fig. 2d. Hence, there are six force fluctuations in Fig. 16b for the specimens with 6 ribs @ 50 mm.

6.4. Effect of epoxy ribs locations

It is of interest to find the effect of the epoxy rib locations on the global response.
Let f_{co} = 35 MPa, d_e = 5 mm, L_r = 30 mm. Five different cases are calculated:

a) Concrete normally bonded by FRP without any epoxy interlocking;
b) Concrete bonded by FRP with 10 epoxy ribs @ 30 mm;
c) Concrete bonded by FRP with 3 epoxy ribs @ 30 mm; the first rib is located at 30 mm from the loaded end;
d) Concrete bonded by FRP with 3 epoxy ribs @ 30 mm; the first rib is located at 120 mm from the loaded end;
e) Concrete bonded by FRP with 3 epoxy ribs @ 30 mm; the first rib is located at 240 mm from the loaded end.

The calculated load-displacement curves, as well as the schematic images, of the five cases above are illustrated in Fig. 17. The load-displacement curves of cases (c), (d) and (e) are located between the cases (a) and (b). In terms of the cases (c), (d) and (e), if the ribs are close to the loaded end, the interlocking effect works initially and later trends to the normal bonded case (case (a)), as shown in Fig. 17. However, if the ribs are located close to the free end, the interlocking effect does not work initially, but works at the end stage before failure.

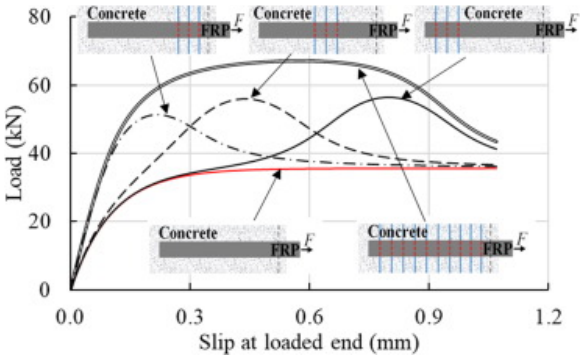

Fig. 17. Effect of locations of epoxy ribs.

7. Conclusions

The concept of a novel approach called epoxy interlocking was proposed in this paper. The adhesive layer can be conducted with many ribs by grooving on the concrete surface before applying epoxy. This concept was proved and the average partial interaction relationship was calibrated by an experimental program. The bond strength of tested epoxy interlocking specimens had a percentage of 88.8% increase compared to the wax filled specimens, due to the epoxy interlocking effect. The partial interaction relationship for individual epoxy rib, which was derived from an analytical approach, showed to be highly related to the concrete compression behavior. Based on the proposed methodology and the analytical model in this paper, a parametric study was conducted on the effects of groove depth and spacing, concrete strength and epoxy rib location. The reasonable results in the parametric study further verify the efficiency of the proposed bond scheme to enhance the bond behavior between FRP and concrete.

Conflict of interest

The authors declared that there is no conflict of interest

Acknowledgements

The first author of this paper obtained financial aids from City University of Hong Kong for his visiting to Marquette University to perform this study. The fourth author was supported by the financial aid from Marquette University during his graduate study. The FRP materials were donated by Fyfe Company LLC.

References

[1] D.M. Zhang, X.L. Gu, Q.Q. Yu, H. Huang, B. Wan, C. Jiang **Fully probabilistic analysis of FRP-to-concrete bonded joints considering model uncertainty** *Compos. Struct*., 185 (2018), pp. 786-806

[2] I. Iovinella, A. Prota, C. Mazzotti **Influence of surface roughness on the bond of FRP laminates to concrete** *Constr. Build. Mater*., 40 (2013), pp. 533-542

[3] J. Xiao, J. Li, Q. Zha **Experimental study on bond behavior between FRP and concrete** *Constr. Build. Mater*., 18 (10) (2004), pp. 745-752

[4] J.R. Cromwell, K.A. Harries, B.M. Shahrooz **Environmental durability of externally bonded FRP materials intended for repair of concrete structures** *Constr. Build. Mater*., 25 (5) (2011), pp. 2528-2539

[5] H. Niu, Z.S. Wu **Effects of FRP-concrete interface bond properties on the performance of RC beams strengthened in flexure with externally bonded FRP sheets** *J. Mater. Civ. Eng*., 18 (5) (2006), pp. 723-731

[6] H. Yuan, J.G. Teng, R. Seracino, Z.S. Wu, J. Yao**Full-range behavior of FRP-to-concrete bonded joints** *Eng. Struct*., 26 (5) (2004), pp. 553-565

[7] A. Hosseini, D. Mostofinejad **Effect of groove characteristics on CFRP-to-concrete bond behavior of EBROG joints: experimental study using particle image velocimetry (PIV)** *Constr. Build. Mater.*, 49 (2013), pp. 364-373
[8] A. Hosseini, D. Mostofinejad **Experimental investigation into bond behavior of CFRP sheets attached to concrete using EBR and EBROG techniques** *Compos. B Eng.*, 51 (2013), pp. 130-139
[9] Y.F. Wu, L. He, L. Bank **Bond-test protocol for plate-to-concrete interface involving all mechanisms** *J. Compos. Constr.*, 20 (1) (2015), p. 04015022
[10] S. Kim, S.T. Smith **Behaviour of handmade FRP anchors under tensile load in uncracked concrete** *Adv. Struct. Eng.*, 12 (6) (2009), pp. 845-865
[11] T. Ozbakkaloglu, M. Saatcioglu **Tensile behavior of FRP anchors in concrete** *J. Compos. Constr.*, 13 (2) (2009), pp. 82-92
[12] S.T. Smith, S. Hu, S.J. Kim, R. Seracino **FRP-strengthened RC slabs anchored with FRP anchors** *Eng. Struct.*, 33 (4) (2011), pp. 1075-1087
[13] H. Zhang, S.T. Smith **Influence of FRP anchor fan configuration and dowel angle on anchoring FRP plates** *Compos. B Eng.*, 43 (8) (2012), pp. 3516-3527
[14] L. Bank, D. Arora **Analysis of RC beams strengthened with mechanically fastened FRP (MF-FRP) strips** *Compos. Struct.*, 79 (2) (2007), pp. 180-191
[15] A.J. Lamanna, L. Bank, D.W. Scott **Flexural strengthening of reinforced concrete beams by mechanically attaching fiber-reinforced polymer strips** *J. Compos. Constr.*, 8 (3) (2004), pp. 203-210
[16] J.A. Martin, A.J. Lamanna **Performance of mechanically fastened FRP strengthened concrete beams in flexure** *J. Compos. Constr.*, 12 (3) (2008), pp. 257-265
[17] P. Zhang, H. Zhu, G. Wu, S.P. Meng, Z.S. Wu **Shear capacity comparison of four different composite interfaces between FRP plates and concrete substrate** *J. Compos. Constr.*, 20 (4) (2016), p. 04016006
[18] Y.F. Wu, Y. Huang **Hybrid bonding of FRP to reinforced concrete structures** *J. Compos. Constr.*, 12 (3) (2008), pp. 266-273
[19] Y.F. Wu, K. Liu **Characterization of mechanically enhanced FRP bonding system** *J. Compos. Constr.*, 17 (1) (2013), pp. 34-49
[20] Y.F. Wu, J.H. Yan, Y.W. Zhou, Y. Xiao **Ultimate strength of reinforced concrete beams retrofitted with hybrid bonded fiber-reinforced polymer** *ACI Struct. J.*, 107 (4) (2010), pp. 451-460
[21] Y.F. Wu, Z.Y. Wang, K. Liu, W. He **Numerical analyses of hybrid-bonded FRP strengthened concrete beams** *Comput.-Aided Civ. Infrastruct. Eng.*, 24 (5) (2009), pp. 371-384
[22] Z.M. Wu, C.H. Hu, Y.F. Wu, J.J. Zheng **Application of improved hybrid bonded FRP technique to FRP debonding prevention** *Constr. Build. Mater.*, 25 (6) (2011), pp. 2898-2905
[23] B. Wan, C. Jiang, Y.F. Wu **Effect of defects in externally bonded FRP reinforced concrete** *Constr. Build. Mater.*, 172 (2018), pp. 63-76
[24] Y.W. Zhou, Y.F. Wu, Y.C. Yun **Analytical modeling of the bond–slip relationship at FRP-concrete interfaces for adhesively-bonded joints** *Compos. B Eng.*, 41 (6) (2010), pp. 423-433
[25] J.F. Chen, J.G. Teng **Anchorage strength models for FRP and steel plates bonded to concrete** *J. Struct. Eng.*, 127 (7) (2001), pp. 784-791
[26] Y.F. Wu, C. Jiang **Quantification of bond-slip relationship for externally bonded FRP-to-concrete joints** *J. Compos. Constr.*, 17 (5) (2013), pp. 673-686
[27] M.B. Ouezdou, A. Belarbi, S.W. Bae **Effective bond length of FRP sheets externally bonded to concrete** *Int. J. Concr. Struct. Mater.*, 3 (2) (2009), pp. 127-131
[28] A. Hosseini, D. Mostofinejad **Effective bond length of FRP-to-concrete adhesively-bonded joints: experimental evaluation of existing models** *Int. J. Adhes. Adhes.*, 48 (2014), pp. 150-158
[29] H. Zhang, S.T. Smith, R.J. Gravina, Z. Wang **Modelling of FRP-concrete bonded interfaces containing FRP anchors** *Constr. Build. Mater.*, 139 (2017), pp. 394-402

[30] C. Jiang, Y.F. Wu, M.J. Dai **Degradation of steel-to-concrete bond due to corrosion** *Constr. Build. Mater*., 158 (2018), pp. 1073-1080

[31] C. Jiang, B. Wan, J. Omboko **Enhancing FRP-to-concrete bond behavior by epoxy ribs** *Proc., the 13th International Symposium on Fiber-Reinforced Polymer Reinforcement for Concrete Structures (FRPRCS-13),* California, USA (2017)

[32] J. Omboko ***Evaluating the bond behavior between FRP and grooved concrete specimens using single shear pull out test*** (Master thesis) Marquette University, WI, USA (2017)

[33] A.M. Neville *Properties of Concrete* (fourth ed.), ELBS Publication, Addison-Wesley Longman Limited, Essex, UK (1996)

[34] C. Jiang, Y.F. Wu, J.F. Jiang **Effect of aggregate size on stress-strain behavior of concrete confined by fiber composites** *Compos. Struct*., 168 (2017), pp. 851-862

[35] J.G. Dai, T. Ueda, Y. Sato **Development of the nonlinear bond stress–slip model of fiber reinforced plastics sheet–concrete interfaces with a simple method** *J. Compos. Constr*., 9 (1) (2005), pp. 52-62

[36] K. Liu, Y.F. Wu **Analytical identification of bond–slip relationship of EB-FRP joints** *Compos. B Eng*., 43 (4) (2012), pp. 1955-1963

[37] Y.F. Wu, C. Jiang **Analytical identification of bond parameters for EB-FRP joints** *Proc., 7th International Conference on FRP Composites in Civil Engineering (CICE2014),* Vancouver, 040 (2014)

[38] Y.F. Wu, X.S. Xu, J.B. Sun, C. Jiang **Analytical solution for the bond strength of externally bonded reinforcement** *Compos. Struct*., 94 (11) (2012), pp. 3232-3239

[39] H.T. Wang, G. Wu **Bond-slip models for CFRP plates externally bonded to steel substrates** *Compos. Struct*., 184 (2018), pp. 1204-1214

[40] Z.C. Girgin, N. Arioglu, E. Arioglu **Evaluation of strength criteria for very-high-strength concretes under triaxial compression** *ACI Struct. J.,* 104 (3) (2007), pp. 278-284

[41] Y.G. Cao, C. Jiang, Y.F. Wu **Cross-sectional unification on the stress-strain model of concrete subjected to high passive confinement by fiber-reinforced polymer** *Polymers*, 8 (5) (2016), p. 186

[42] Y.F. Wu, C. Jiang **Effect of load eccentricity on the stress–strain relationship of FRP-confined concrete columns** *Compos. Struct*., 98 (2013), pp. 228-241

[43] S. Popovics **Numerical approach to the complete stress–strain relation for concrete** *Cem. Concr. Res*., 3 (5) (1973), pp. 583-599

[44] ACI Committee 318 ***Building Code Requirements for Structural Concrete and Commentary (ACI 318-99)*** American Concrete Institute, Detroit, MI (1999)

[45] D.J. Carreira, K.H. Chu **Stress-strain relationship for plain concrete in compression** *ACI J*., 82 (6) (1985), pp. 797-804

[1]Formerly, Visiting Scholar, Marquette University, Milwaukee, WI 53201, United States.